Inverse Simulation System for Evaluating Handling Qualities During Rendezvous and Docking

Wanmeng Zhou[a], Hua Wang[a*], Douglas Thomson[b], Guojin Tang [a], Fan Zhang [a]

[a]*College of Aerospace and Engineering, National University of Defense Technology, Changsha 410073, China*

[b]*School of Engineering, University of Glasgow, Glasgow, G12 8QQ, UK*

[*] Corresponding author: Tel.: +8613973104555; Email address: wanghua@nudt.edu.cn

Abstract

The traditional method used for handling qualities assessment of manned space vehicles is too time-consuming to meet the requirements of an increasingly fast design process. In this study, a rendezvous and docking inverse simulation system to assess the handling qualities of spacecraft is proposed using a previously developed model-predictive-control architecture. By considering the fixed discrete force of the thrusters of the system, the inverse model is constructed using the least squares estimation method with a hyper-ellipsoidal restriction, the continuous control outputs of which are subsequently dispersed by pulse width modulation with sensitivity factors introduced. The inputs in every step are deemed constant parameters, and the method could be considered as a general method for solving nominal, redundant, and insufficient inverse problems. The rendezvous and docking inverse simulation is applied to a nine-degrees-of-freedom platform, and a novel handling qualities evaluation scheme is established according to the operation precision and astronauts' workload. Finally, different nominal trajectories are scored by the inverse simulation and an established evaluation scheme. The scores can offer theoretical guidance for astronaut training and more complex operation missions.

Key Words: Rendezvous and docking; inverse simulation system; handling qualities; Cooper–Harper ratings

---

Abbreviations:
DISS: Discrete inverse simulation system
MPC: Model predictive control
RVD: Rendezvous and docking

1. Introduction

Rendezvous and docking (RVD) refers to the event in which two spacecraft encounter each other at nearly the same velocity and dock together [1]. Due to the sophisticated and complex nature of a spacecraft, the automatic control system that manages RVD might face failures which, along with the uncertainty of the space environment, might lead to mission failure. A manual control system can act as a backup for the automatic control system and hence decreases the risk of mission failure. Though there is a trend to rely more on the automatic control system, the option of manual control is still required in manned space missions for proximity operations and docking [2].

Handling qualities are those characteristics of a flight vehicle that govern the ease and precision with which a pilot is able to perform a flying task [3]. In a man-in-loop system, handling qualities are used to characterise the control regulated by the human. Handling qualities evaluation is carried out using both analytical and experimental methods [4–6]. In the field of aeronautics, early systems were designed using analytical methods; subsequently, experimental methods were developed gradually. The former methods focus on pilot modelling: changing the pilot model parameters in the frequency domain to study the pilot's ability to compensate for the failures. McRuer et al. conducted early research on pilot modelling [7]. Neal and Smith summarised the results of former studies and proposed the well-known Neal–Smith model combined with a handling qualities rating scale for the frequency domain analysis of a human-in-the-loop system [8]. Kleinman, Baron, and Levison proposed an optimal control model [9], and Schmidt, Doman, and Anderson proposed further refinements to this model, resulting in increasingly accurate optimal control models [10,11]. Hess found a linear relationship between the objective function and handling qualities, according to which he predicted the flight vehicle handling qualities [12]. Thomson et al. employed an inverse simulation method to construct a helicopter simulation system that could perform initial handling qualities assessments [13,14].

In the field of astronautics, most studies on handling qualities tend to adopt experiment methods [15,16]. Designers utilise experimental platforms to simulate aerospace missions and record astronauts' sensations. To reduce the effects of individual differences and random factors, experiment designers train astronauts repeatedly and account for their cultural backgrounds, subjective positivity, and mental states. Because of these procedures, experimental methods are time-consuming, and the estimations from astronauts depend largely on subjective sensations, which cannot provide suggestions for improving operations. However, evaluation systems continue to use Aeronautical Design Standard rating scales such

as the Cooper–Harper rating scale [17] and Task Load Index [18]. Therefore, an effective evaluation method for rating handling qualities when no operators participate in the initial design stage would be useful. The research reported in this document proposes to address this issue by developing an inverse simulation method for application to the RVD task that can reproduce astronauts' control strategies. By relating the simulation results to handling qualities metrics, the method can yield a quantitative evaluation of handling qualities that forms the basis of an assessment for initial system designs.

As the name implies, inverse simulation is a technique used to calculate the control action required to achieve a specified system response (such as pilot operations in the case of this study) [19]. Inverse simulation theory was first developed as a tool for aircraft dynamics analysis. Experimentally measured data or a mathematical representation can be used to simulate a particular mission, and a dynamic model of the system of interest used to compute the response and control strategies required to complete the mission. Inverse simulation has been referred to as 'desktop flight testing' [19]. The main applications of the theory include standard pilot modelling, aircraft model validation, handling qualities evaluation, and flight configuration studies. A differentiation method was first adopted to calculate the desired outputs [20,21]. Subsequently, Hess, Gao, and Wang proposed an integration method [22,23] to avoid the complexity and model restructuring required for the differentiation method, which was being widely used. The method was utilised by Thomson et al. to study helicopter manoeuvre performance and further develop the system for assessing handling qualities and planning breakdown operation schemes [24]. Later, the two-timescale method [25] and global optimization method [26] were proposed, both of which were based on the integration method. To decrease the computational cost, Avanzini, Thomson, and Torasso introduced a model-predictive-control architecture for the inverse simulation that improved the efficiency of the previous inverse simulation systems [27]. This architecture is the basis for the RVD inverse simulation system proposed in this paper. During the RVD manoeuvre, the motion states of the chaser spacecraft must be precisely controlled to guarantee that the target spacecraft remains in the sensor view. Control actions are executed by thrusters, which apply constant amplitude pulses. Therefore, in contrast to general inverse problems, the control signal of this system is discrete and the dimension of the motion states are larger than those of the control inputs.

This paper first proposes models for a spacecraft's relative orbit and attitude motion. The discrete inverse simulation (DIS) method is then constructed based on these models using a model-predictive-control architecture. Based on this system, which is verified by experimental data from a nine-degrees-of-

freedom (9-DOF) RVD platform, and previous handling qualities rating scales, an improved assessment scheme is proposed to study the handling qualities of different mission configurations.

2. Inverse System Modelling of RVD

2.1 Modelling of Relative Motion of Spacecraft

The absolute dynamic equations between the target spacecraft and chase spacecraft without any hypothesis can be expressed as

(1)

(2)

where the subscripts *tar* and *cha* represent the target and chaser spacecraft, respectively; $\boldsymbol{a}$ is the acceleration caused by the external force, mainly the thrust of actuators here; R_{tar} and R_{cha} are the distance between the Earth's center and the target and chaser, respectively; μ and t are the standard gravitational parameter and time, respectively. The components of relative equations are given by

(3)

where ω is the angular velocity, and a_{fx}, a_{fy}, and a_{fz} are the components of $\boldsymbol{a}_{cha} - \boldsymbol{a}_{tar}$ in the Hill coordinate system, respectively. The functions can be simplified by making the following acceptable assumptions [28]: the Earth is a homogeneous sphere; gravitational perturbation can be ignored; the orbit of the target is circular, and the distance between the target and chaser is much less than the target orbital radius. Therefore, the Hill coordinate system illustrated in Fig. 1 and Eq. (3) can be simplified as

(4)

where u is the input control component in the Hill coordinate system. Eq. (4) can be further transformed into state equations.

(5)

where $\boldsymbol{\Phi}(t,t_0)$ is the state transition matrix and $\boldsymbol{\Phi}_{\boldsymbol{u}}(t,t_0)$ is the input transition matrix. These matrices are expressed in Eq. (6) and Eq. (7), respectively:

(6)

(7)

where $\Delta t = t - t_0$, $s = \sin\omega\Delta t$, and $c = \cos\omega\Delta t$.

When the inputs are constant within a step, Eq. (5) can be expressed as

(8)

where $\bar{\boldsymbol{\Phi}}_{\boldsymbol{u}}(t,t_0)$ is given by

(9)

The expected control input $\boldsymbol{u}^*$, is represented in terms of the Hill coordinate system as

(10)

where $\boldsymbol{C}_{\boldsymbol{hb}}$ is the transformation matrix from the Hill coordinate system to the body coordinate system and can be expressed as

(11)

where ϕ, θ, ψ are roll, yaw, and pitch angles, respectively.

When the relative attitude deviation between the chaser and target is exiguous, Eq. (11) can be simplified to

(12)

The attitude dynamics equation of the spacecraft, based on the general rigid rotation equations, is expressed as

(13)

where $\boldsymbol{I}$, $\boldsymbol{M}$, and $\boldsymbol{\omega}$ are the moment of inertia, external torque, and angular velocity of the spacecraft, respectively. When $\boldsymbol{I}$ is a diagonal matrix, Eq. (13) can be expressed as

(14)

The attitude kinematic function can be expressed as

(15)

The structure of IS for both translational and rotational motions is more complex than that of IS only for translational motion. Further, an IS method for coupled attitude and orbit dynamics would raise many additional issues that may distract from the main points of this research. Thus, in this study, during the RVD process, the orbit is controlled manually, whereas the attitudes of the chaser and target are controlled automatically. The IS structure of orbit control can be regarded as a basic of 6-DOF control, which has some potential applications such as spacecraft tracking and satellite automatic formation.

2.2 Discrete Inverse Simulation Modelling

DIS includes a data or guidance block, an inverse model block, a forward simulation block, and a parameter measurement block. This structure is similar to that of model predictive control (MPC). The DIS incorporates the online and multivariable control advantages of MPC; furthermore, it can guarantee accuracy and overall efficiency when using the simplified inverse model and high-precision forward model. The main difference is whether the solved control sequence along the receding horizon is constant or not [29]. The relationships between these blocks are shown in Fig. 2.

Traditional inverse simulation methods such as differentiation and integration focus on problems in

continuous-time systems; however, the operation modes of the manually controlled RVD system are discrete. Therefore, a zero-order holder is added in the inverse model block.

In the DIS data flow, the inverse model block is the interior loop and other blocks compose the external loop. The output variables here are the components of trajectories and velocities, which are the same as the state variables. Thus, the "expected state" is used hereafter as a substitute for the desired output variables. In Fig. 2, $\hat{\boldsymbol{x}}(t+\Delta t)$ is the measured current state of the spacecraft, which is produced by the measurement block; $\boldsymbol{x}(t+n\Delta t)^*$ is the expected state, which is produced by the experimental data or a guidance law block; $n\Delta t$ is the receding horizon of the inverse model block, and n is the number of simulation steps. The desired control input u^* can be calculated according to the current state $\hat{\boldsymbol{x}}(t+\Delta t)$ and expected state $\boldsymbol{x}(t+n\Delta t)^*$. Subsequently, u^* is transmitted to the forward simulation block, and the updated data are then obtained and transmitted into the next loop.

The method to calculate the desired control input is given below. According to Eq. (8). The state transition matrix in limited steps can be expressed as

(16)

Reorganizing Eq. (16), the final state of the limited steps can be expressed as

(17)

where the input assemblage $\hat{\boldsymbol{U}}$ and matrix $\boldsymbol{\Phi}^*$ are given by

(18)

(19)

When $\bar{\boldsymbol{\Phi}}_u$ is constant during the forward steps of the inverse simulation. Eq. (17) can then be simplified as

(20)

where $\hat{\boldsymbol{u}}$ is the control input and $\boldsymbol{\xi}$ can be expressed as

(21)

Considering the initial state deviations, the state function is expressed as

(22)

where $\boldsymbol{\varepsilon}$ represents the state deviation, the expectation $E(\boldsymbol{\varepsilon}) = \boldsymbol{0}$, and the variance $E(\boldsymbol{\varepsilon}\boldsymbol{\varepsilon}^T) = \boldsymbol{\sigma}$. Further, when the step size is fixed, Eq. (22) can be expressed as

(23)

Eq. (24) and Eq. (25) are derived based on the features of the state transition matrix:

(24)

(25)

The mathematical form expressed in Eq. (23) can be classified into three types: *nominal*, where the number of inputs is equal to the number of outputs; *redundant*, where the number of input dimensions is greater than the number of output dimensions; and *underactuated*, where the number of input dimensions is less than the number of output dimensions. The dimensional relationship between $\boldsymbol{x}(n+k)$ and $\boldsymbol{u}(k)$ can represent the different types. For nominal problems, $\boldsymbol{u}(k)$ can be calculated algebraically; for redundant and underactuated problems, the equations need to be further transformed as follows.

Inverse simulation seeks the best input $\boldsymbol{u}^*$ to minimize the deviations between the expected and predicted values; the deviations can be expressed as

(26)

where $\boldsymbol{x}$ is the predicted value; $\boldsymbol{x}^*$ is the expected values or the measured data; and $\boldsymbol{Q}$ is the weighting coefficient matrix, which reflects the weight of state deviations. Substituting Eq. (23) into Eq. (26), the deviations can be expressed as

(27)

The solutions for the minimised $J(\boldsymbol{u}(k))$ can be obtained whether Eq. (23) is compatible or not. According to the theory of the generalized inverse matrix, the minimum norm least squares solution can be given as

(28)

3. Simulation and Validation

3.1 Manually Controlled RVD Simulation Platform

An experimental platform is required to validate the inverse system model. In the United States, NASA's Langley Research Centre used the Apollo simulation capsule to research handling qualities prior to the astronaut moon-landing mission [30]. NASA's Ames Research Centre utilised the Orion simulation platform [31] to study handling qualities under different control models by simulating the RVD process between the crew exploration vehicle and the International Space Station.

All experimental data reported in this paper are generated from a man-in-loop experimental platform referred to as the 9-DOF manually controlled RVD platform [32], which is located at the National University of Defense Technology in China, shown in Fig. 3.

The experimental system [33] consists of a 9-DOF motion platform, an operation console, a visualization subsystem, and a simulation subsystem. The chaser model and the target model both have 3-DOF in rotational motions, and the slideway has 3-DOF in translational motions. The operation of the hand sticks can be transformed into the motion control signal through the RS232 and digital signal processor (DSP) from the operations console. The sensor image acquisition device updates the pictures in the display terminal through the video graphics adapter (VGA). The simulation subsystem loaded on DSP calculates the relative motions in accordance with the model given in this paper. This system is able to demonstrate a manually controlled RVD process and is different from the all-digital simulation systems used at Langley and Ames. Operators can observe the RVD process through a video graphics array and control the chaser using sticks from the console. The digital signal processor transforms the operation into signal data, and the data are then transmitted to the motion control devices. The processor can record all the manual operations during the experiment.

3.2 RVD Inverse Simulation System Validation

The data on the astronauts' operations and RVD trajectories are acquired from the 9-DOF manually controlled RVD platform. The inverse simulation system can then be validated by reproducing the data on manoeuvres and experimental operations.

The simulation step, the receding horizon, and the sensitivity factor k are set to be 1, 3, and 0.4, respectively. Ignoring the measurement deviation and installation deviation, the target function weight coefficient matrix $\boldsymbol{Q}$ is simply defined as $\boldsymbol{I}$. The initial relative states of the spacecraft models are set as $x_{c0} = 100.038$ m, $y_{c0} = -0.023$ m, $z_{c0} = -0.0167$ m, and $v_{x0} = 0.00756$ m/s. Fig. 4 illustrates the manually controlled RVD trajectories produced by the experiment and inverse simulation. The results for

the velocity and control signals in the *x*, *y*, and *z* axes are shown in Fig. 5. The experiment results were produced by the man-in-loop platform and all the control actions were executed by the operator. The recorded trajectory can be considered as the desired outputs, and the IS method is shown to reproduce the pulses successfully in accordance with the practical operation. These results indicate that the RVD inverse simulation system can reproduce the operator's actions, especially for the intensive manoeuvreing periods. It should be noted that the traditional control method can also track the experimental data, but it yields inaccurate manoeuvre results because its closed-loop feedback mechanism does not reflect the actual situation [34].

4. RVD Inverse Simulation Applications

4.1 Inverse Simulation System Design

The measures taken to make the proper choices for the simulation step, receding horizon, and sensitive factors for the modelling process are explained in this section.

The input of the DIS is considered to be the step signal in each simulation step. The choice of the simulation step has no influence on the steady-state error of the system but can affect the simulation's precision in each step and the computational time. According to previous analysis, using the sample step as the simulation step can always satisfy the requirements of precision and computational time [34]. A general receding horizon is selected to be between 3 and 5 because smaller or larger receding horizons would cause the instability of the system and a large receding horizon can increase the computational cost [35].

The sensitivity factor reflects the sensitivity of the inverse simulation system to state errors. A large sensitivity factor means that the errors must be sufficiently large to cause the activation of actuators, whereas a small sensitivity factor means that a small error can cause the activation of actuators. To confirm these sensitivity factors, five experiments were performed with sample steps of 0.1s. Ten inverse simulations, each with a different factor, were performed based on each group of experimental data. The mean process deviation and pulse number deviation are expressed as

(29)

where x_i is the simulation state, $\tilde{x}_i$ is the experimental state, T_n is the simulation number of pulses , and $\tilde{T}_n$ is the experimental number of pulses . The average deviations of the number of pulses , positions and velocities are illustrated in Figs. 6 to 8, respectively.

From the above results, we can conclude that the system's sensitivity factor has a minor effect on the average velocity deviations. Therefore, only the average position and number of pulses are considered to determine the sensitivity factor of the system.

The number of pulses decrease as the sensitivity factors become larger, and this number continuously approach a finite value. Because of measurement errors, the deviation of the position appears to fluctuate but nonetheless reveals an overall increasing trend as the sensitivity factors become larger. Considering the number of pulses and position deviations, the proper inverse simulation sensitivity factor is found to be between 0.3 and 0.5. Therefore, the system's simulation step and sensitivity factor are set to be 0.1 s and 0.35, respectively, to optimize the precision to the greatest extent possible.

4.2 Evaluation Scheme Based on the Cooper–Harper Rating Scale

Using the validated system, the handling qualities of specific missions can be evaluated based on the impact position deviations and overall number of pulses , which reflect the performance and ease of operating the spacecraft in the Cooper–Harper rating scale. Therefore, to use the inverse system as a tool for initial handling qualities assessments, the relationships between the Cooper–Harper rating and inverse simulation results must first be established.

According to the description of the Cooper–Harper ratings [17], the handling qualities of the system are determined by the final performance and operators' compensation. The ratings first evaluate the controllability of the system and then determine the precision and compensation provided by the operator, as shown in Fig. 9.

For a manually controlled RVD, performance is represented by the final impact positions and velocities, which are scored on the Cooper–Harper rating scale by different precision values. The limitations on these impact states are expressed as

(30)

where $k_i, l_i \ (i = 1, 2, 3)$ refer to the precision of the positions and velocities, respectively, in different levels. The rating for compensation utilises the total pulse percentage of the basic pulse amounts. The ease of the mission is reflected by the operators' compensation, which is defined as an operation ratio and expressed as

(31)

where f_{thrust} is the basic number of pulses in one axis; f is the number of pulses in the simulation ; and kf_A, kf_B, and kf_C represent the operation ratios of Grades A, B, and C, respectively.

The inverse simulation system assesses the handling qualities of a mission in a similar manner to the Cooper–Harper rating scale, as listed in Table 1.

Table 1

RVD handling qualities assessment ratings.

Rating	A $kf \le kf_A$	B $kf_A \le kf \le kf_B$	C $kf_B \le kf \le kf_C$
Level 1 $\sqrt{\Delta Y^2 + \Delta Z^2} \le k_1$ $\lvert\Delta V_Y\rvert \le l_1, \lvert\Delta V_Z\rvert \le l_1$	1. Desired Precision with Little Compensation	2. Desired Precision with Extensive Compensation	3. Desired Precision with Intense Compensation
Level 2 $\sqrt{\Delta Y^2 + \Delta Z^2} \le k_2$ $\lvert\Delta V_Y\rvert \le l_2, \lvert\Delta V_Z\rvert \le l_2$	4. Adequate Precision with Little Compensation	5. Adequate Precision with Extensive Compensation	6. Adequate Precision with Intense Compensation
Level 3 $\sqrt{\Delta Y^2 + \Delta Z^2} \le k_3$ $\lvert\Delta V_Y\rvert \le l_3, \lvert\Delta V_Z\rvert \le l_3$	7. Controllable Precision with Little Compensation	8. Controllable Precision with Extensive Compensation	9. Controllable Precision with Intense Compensation

The inverse simulation assessment ratings are different from the Cooper–Harper ratings in that performance is a top priority factor, and therefore, achieving the desired precision with intense compensation can earn a high rating. The final ratings satisfying the limitation of Level 1, represented by ratings 1–3 for little compensation to intense compensation, indicate that the mission can achieve the desired precision. The other levels earn ratings in the same manner. When the performance is outside the limitation of Level 3 or when compensation beyond Grade C is required, the uncontrollable situations correspond to a rating of 10 on the Cooper–Harper rating scale.

4.3 Initial Handling Qualities Assessment

Based on the above assessment schemes, ratings for the in-track [36] and cross-track [37] nominal trajectories can be evaluated prior to the assessment of handling qualities.

4.3.1 In-track Nominal Trajectory Design

The forbidden zone has the shape of a sphere or a rectangular parallelepiped centered about the target's centroid and it is defined to avoid collisions between two spacecraft and protect the target sensor from

pollution generated by the plume. Depending on whether an evading manoeuvre exists or not, the safety mode is divided into the active safety mode, which consumes more fuel, and the passive safety mode, which reduces the approach speed as the target gets closer. If the chaser is operated in the active safety mode at the beginning, it will consume more fuel to accelerate in the reverse direction at the end. Based on these considerations of time and fuel consumption, a guidance law combining the passive and active safety modes was designed, as illustrated in Fig. 10.

The chaser first runs in the passive safety mode, and the speed of the chaser increases to a particular speed v_0; subsequently, the chaser maintains uniform motion and then begins to index brake at x_1. During the braking process, the mode of the chaser switches from the passive mode to the active mode at x_2. Index braking refers to linearly decreasing the velocity relative to the decreasing distance between the target and chaser; this relationship is expressed as $v = kx + v_1$, where k is the slope and $k = \frac{v_0 - v_t}{x_0 - x_t} < 0$. The chaser is located at x_1 moving at the speed v_0 in the beginning and is located at x_t moving at the speed v_t at the end. From this relationship, the index curve can be expressed as

(32)

The entire time from x_0 to the completion of the RVD manoeuvre is determined by $T = \frac{1}{k} \ln \frac{v_t}{v_0}$.

The chaser begins uniform motion at the initial position x_0 and initial velocity v_0. The switching time of the guidance law is expressed as $t_0 = (x_0 - x_1) / v_0$, where x_1 is the switching point. Because the final position and velocity approach zero, the slope $k = \frac{v_0}{x_0} < 0$. Based on Eq. (32), the cross-track guidance law is expressed as

(33)

4.3.2 Cross-track Nominal Trajectory Design

The cross-track nominal trajectory can be obtained using the average experimental data shown in Fig. 11.

The determination of the manually controlled trajectory is similar to the reduction of a trigonometric function [37], which is expressed as

(34)

where the amplitude A reflects the initial deviation, the reduction index α refers to the convergence speed of the cross-track deviation, and the frequency w reflects the sensitivity of the operator. According to Eq. (4), the motion in the y-axis direction is independent of the motion in the direction of the other axes, and only the motion in the x-axis direction influences the motion in the z-axis direction. Therefore, the simulation cases proposed in this paper were defined by the fixed in-track nominal trajectory and various nominal cross-track trajectories to gain insight into the operation.

An effective operation scheme is to decrease the deviation directly in the beginning. Therefore, the initial phase constraint is $\varphi \in [0^{\circ}, 90^{\circ}) \cup [180^{\circ}, 270^{\circ})$. To compare the effects of different motion parameters on manually controlled RVD processes, the reduction of the trigonometric function expressed by Eq. (34) is required to satisfy both the initial and terminal position constraints:

(35)

Based on the positions and phase constraints defined in this manner, 10 nominal cross-track trajectories are designed, as listed in Table 2.

Table 2

Different cross-track nominal trajectories.

No.	y-axis Amplitude (m)	z-axis Amplitude (m)	Phase (°)	Frequency (rad/s)	Index Parameter
1	0.4785	0.659	88	0.0484	0.004
2	0.9569	1.3179	89	0.0483	0.004
3	1.9137	2.6356	89.5	0.0483	0.004
4	-0.9569	-1.3179	269	0.0459	0.004
5	1.9137	2.6356	89.5	0.0242	0.004
6	1.9137	2.6356	89.5	0.0145	0.004
7	1.9137	2.6356	89.5	0.0725	0.004
8	1.9137	2.6356	89.5	0.0483	0.003
9	1.9137	2.6356	89.5	0.0483	0.005
10	1.9137	2.6356	89.5	0.0483	0.007

In Nos. 1–3 the amplitudes are changed and in Nos. 2 and 4 the frequencies are changed, at the same time, the phases are adjusted accordingly. In Nos. 5–7, the trajectory frequencies are changed, and in Nos. 8–10, the index parameters are changed. According to Eq. (34), the trajectories cannot achieve the initial

and final positions and velocities simultaneously, but when the final position is submitted to the constraints, the terminal velocity would be small enough to satisfy the final docking requirements. Each trajectory is tracked 10 times by the system under the conditions listed in Table 3.

Table 3

Simulation conditions.

Simulation Parameters	Values
Initial Relative Positions	$x=100.038m, y=-0.0167m, z=-0.023m$
Initial Relative Velocities	$vx=-0.0076\,m/s, vy=0.131m/s, vz=-0.0087\,m/s$
Operation Ratios	$kf_A=0.5, kf_B=1, kf_C=1.5$
Basic Pulse Amounts	$f_{thrust}=1000$
Impact Position Precision	$k_1=0.05, k_2=0.08, k_3=0.1$
Impact Velocity Precision	$l_1=0.005, l_2=0.008, l_3=0.01$
RVD Duration	1300 s
Sensitivity Parameter	0.35
Receding Horizon	3
Step	1

The impact distribution and handling qualities assessments are illustrated in Fig. 12 and Fig. 13, respectively. All the terminal velocities satisfy the docking requirements; therefore, the position deviations and number of pulses are set to be the main factors for the performance evaluation.

The results shown in Fig. 12 indicate that all the impacts are in the range of Level 2. Furthermore, most of them are in the range of Level 1. Regarding the number of pulses , most of the trajectories are classified as Grade A except for Nos. 7 and 8. The average ratings of handling qualities obtained from the results are listed in Table 4.

Table 4

Average ratings of handling qualities for different trajectories。

No.	Impact Deviation (m)	Velocity Deviation (m/s)	Operation Ratio	Rating
1	0.03	0.00044	0.423	1
2	0.0382	0.00046	0.424	1
3	0.0528	0.00072	0.496	5
4	0.0523	0.00033	0.461	4
5	0.0346	0.00033	0.432	1
6	0.0427	0.00100	0.471	1

7	0.0357	0.00049	0.746	2
8	0.0536	0.00310	0.535	5
9	0.0449	0.00054	0.487	2
10	0.0348	0.00023	0.449	1

The ratings for No. 3 and Nos. 5–7 indicate that the number of pulses increases with increasing frequency *w*. From the results of No. 3 and Nos. 8–10, we conclude that the increasing index parameter α can increase both the number of pulses and impact deviations. The same is true for the increasing amplitudes. Thus, the deviations and number of pulses would also rise with increasing amplitude or frequency caused by changing phases.

According to the analysis of results, astronauts should eliminate the deviation as quickly as possible to guarantee sufficient time for the terminal adjustment. In addition, astronauts should decrease the frequency to achieve higher precision.

5. Conclusion

In this study, an inverse simulation system based on the characteristics of manually controlled RVD is established, which can be used for the initial assessments of handling qualities. The ratings of handling qualities and the assessment scheme were quantified based on the impact deviations and operation ratios, which reflect the mission performance and the workload of the astronauts, respectively. According to the proposed inverse simulation and the rating scheme, the evaluation results of different nominal trajectories suggested that astronauts should reduce the cross-track deviations quickly to leave sufficient time for final tuning and should decrease the operation frequency to achieve higher mission precision with a reduced number of pulses.

However, it should be noticed that the main purpose of this paper is to exam the possibility of applying inverse simulation in RVD initial handling qualities assessment. Thus, in order to complete the handling qualities assessment and prove its feasibility, some simplifications and assumptions were made during the research. The relative translational motion was represented by a C-W function and the attitude was controlled by another automatic method. The advantage of inverse simulation in controlling nonlinear problems may not yet be apparent, but this is the first step of the research. In the future research, it is hoped to study the establishment of a six-degrees-of-freedom inverse simulation system. The completed system can be used not only in linear problems but also in other nonlinear problems. In addition, designers can

effectively apply the assessment scheme to astronaut training for increasingly complex manually controlled missions.

Conflict of interest statement

The authors declare there is no conflict of interest regarding the publication of this paper.

Acknowledgments

We are grateful to Dr. Douglas Thomson's advice about the improvement of this paper thoroughly, to the participants who volunteered for our experiments, and to the anonymous reviewers for their invaluable feedback. This study was co-supported by the 973 Program (No. 2013CB733100) and the National Natural Science Foundation of China (Nos. 11272346 and 11472301).

References

[1] Y. Z. Luo, J. Zhang, G. J. Tang, Survey of orbital dynamics and control of space rendezvous, Chinese J. Aeronaut. 27 (1) (2014) 1–11.

[2] J. P. Stephens, G. A. Vos, K. D. Bilimoria, E. R. Mueller, J. Brazzel, P. Spehar, Orion handling qualities during international space station proximity operations and docking, J. Spacecraft Rockets. 50 (2) (2013) 449–455.

[3] R. P. Harper, G. E. Cooper, Handling qualities and pilot evaluation, J. Guid. Control Dyn. 9 (5) (1986) 515–528.

[4] D. G. Mitchell, D. B. Doman, D. L. Key, D. H. Klyde, D. B. Leggett, D. J. Moorhouse, D. H. Mason, D. L. Raney, D. K. Schmidt, Evolution revolution and challenges of handling qualities, J. Guid. Control Dyn. 27 (1) (2004) 12–28.

[5] D. T. McRuer, E. S. Krendel, Mathematical models of human pilot behaviour, AGARD-AG-188, 1974.

[6] R. Bradley, G. Turner, G. Brindley, Simulation of pilot control activity for the prediction of workload ratings in helicopter/ship operations, 26th European Rotorcraft Forum, The Hague, Netherlands, 2000.

[7] D. McRuer, D. Graham, E. Krendel, W. Reisenser, Human pilot dynamics in compensatory systems. AFFDL-TR-65-15, 1965.

[8] T. P. Neal, R. E. Smith, An in-flight investigation to develop control system design criteria for fighter airplanes, AFFDL-TR-70-74, 1970.

[9] D. L. Kleinman, S. Baron, W. H. Levison, An optimal control model of human response, Pt. I & II, Automatica. 6 (1970) 357–383.

[10] D. K. Schmidt, Optimal flight control synthesis via pilot modelling, J. Guid. Control Dyn. 2 (4) (1979) 308–312.

[11] D. B. Doman, M. R. Anderson, A fixed-order optimal control model of human operator response, Automatica. 36 (2000) 409–418.

[12] R. A. Hess, Prediction of pilot opinion ratings using an optimal pilot model, Hum. Factors. 19 (1977) 459–475.

[13] D. G. Thomson, R. Bradley, The use of inverse simulation for preliminary assessment of helicopter handling qualities, Aeronaut. J. (1997) 101.

[14] N. Cameron, D. G. Thomson, D. J. Murray-Smith, Pilot modelling and inverse simulation for initial handling qualities assessment, Aeronaut. J. 2792 (2003) 511–520.

[15] K. D. Bilimoria, E. R. Mueller, Frost C R, Handling qualities evaluation of piloting tools for spacecraft docking in earth orbit, J. Spacecraft Rockets. 48 (5) (2011) 846–855.

[16] R. E. Bailey, E. B. Jackson, J. J. Arthur, Handling qualities implication for crewed spacecraft operations, IEEE Aerospace Conference Proceedings, 2012.

[17] G. E. Cooper, R. P. Harper, Use of pilot rating in the evaluation of aircraft handling qualities, NASA TN D-5153, 1969.

[18] S. G. Hart, L. E. Staveland, Development of NASA-TLX (task load index): results of empirical and theoretical research, Human Mental Workload. P.A. Hancock and N. Meshkati (Eds.), North Holland Press, Amsterdam, The Netherlands, 1988.

[19] D. G. Thomson, R. Bradley, Inverse simulation as a tool for flight dynamics research—principles and applications, Prog. Aerosp. Sci. 42 (3) (2006) 174–210.

[20] G. Meyer, L. Cicolani, Application of nonlinear systems inverse to automatic flight control systems design, Theory and Application of Optimal Control in Aerospace Systems, 1981.

[21] H. Haverdings, Improved pilot model for application to a computer flight testing program for helicopters, Proceedings of the 9th European Rotorcraft Forum, Stresa, Italy, 1983.

[22] R. A. Hess, C. Gao, S. H. Wang, Generalized technique for inverse simulation applied to aircraft manoeuvres, J. Guid. Control Dyn. 14 (5) (1991) 920–926.

[23] R. A. Hess, C. Gao, A generalized algorithm for inverse simulation applied to helicopter manoeuvring flight, J. Am. Helicopter Soc. 38 (4) (1993) 3–15.

[24] D. G. Thomson, C. D. Taylor, N. Talbot, R. Ablett, R. Bradley, An investigation of piloting strategies for engine failures during take-off from offshore platforms, Aeronaut. J. 99 (981) (1995) 15–25.

[25] G. Avanzini, G. D. Matteis, Two-timescale inverse simulation of a helicopter model, J. Guid. Control Dyn. 24 (2) (2001) 330–339.

[26] M. Borri, C. L. Bottasso, F. Montelaghi, Numerical approach to inverse flight dynamics, J. Guid. Control Dyn. 20 (4) (1997) 742–747.

[27] G. Avanzini, D. Thomson, A. Torasso, Model predictive control architecture for rotorcraft inverse simulation, J. Guid. Control Dyn. 36 (1) (2013) 207–217.

[28] W. H. Clohessy, R. S. Wiltshire, Terminal guidance system for satellite rendezvous, J. Aerospace Sci. 27 (5)

(1960) 653–674.

[29] D. Q. Mayne, J. B. Rawlings, C. V. Rao, P. O. M. Scokaert, Constrained model predictive control: stability and optimality, Automatica. 36 (6) (2000) 789–814.

[30] D. C. Cheatham, C. T. Hackler, Handling qualities for pilot control of Apollo lunar-landing spacecraft, J. Spacecraft Rockets, 3 (5) (1966) 632–638.

[31] J. P. Ruiz, J. Hart, A comparison between orion automated and space shuttle rendezvous techniques, AIAA Guidance, Navigation, and Control Conference, Toronto, 2010.

[32] J. Y. Zhou, J. P. Zhou, Z. C. Jiang, H. Y. Li, Investigation into pilot handling qualities in teleoperation rendezvous and docking with time delay, Chinese J. Aeronaut. 23 (2) (2012) 622–630.

[33] J. Y. Zhou, Research on concepts and key techniques of teleoperation rendezvous and docking, Ph.D. Thesis, National University of Defense Technology, Changsha, China, 2013.

[34] W. M. Zhou, H. Wang, Research on inverse simulation’s applications in teleoperation RVD based on hyper-ellipsoidal restricted MPC-IS structure, P. I. Mech. Eng. G–JAER. 229 (9) (2014) 1675–1689.

[35] W. M. Zhou, H. Wang, D. T. Yu, F. Y. Sun, Error analysis and modification of inverse simulation for manually controlled rendezvous and docking, J. Aerosp. Eng. 30 (1) (2017) 04016072-1–04016072-9.

[36] H. Wang. Control and trajectory safety of rendezvous and docking, Ph.D. Thesis, National University of Defense Technology, Changsha, China, 2007.

[37] B. Zhang, H. Y. Li, and G. J. Tang, Human control model in teleoperation rendezvous, Sci. China Inf. Sci. 57 (11) (2014) 112205.1–112205.11.

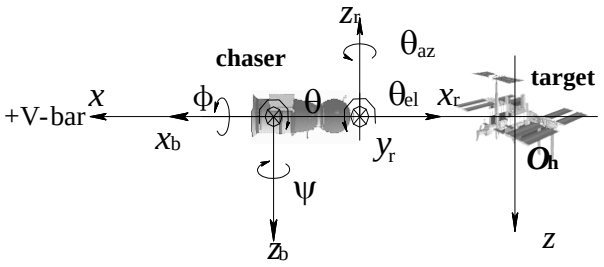

Figure 1 Hill and body coordinate systems

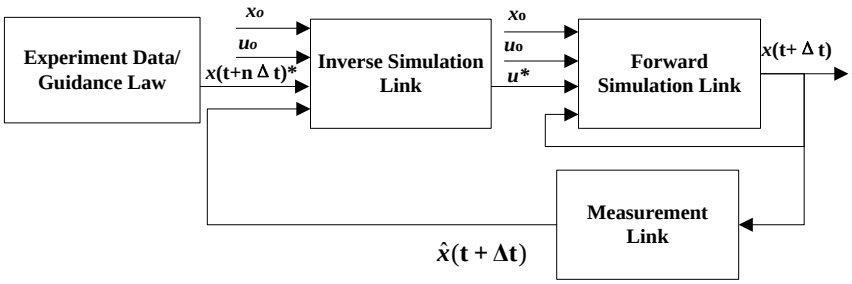

Figure 2 Inverse simulation system architecture

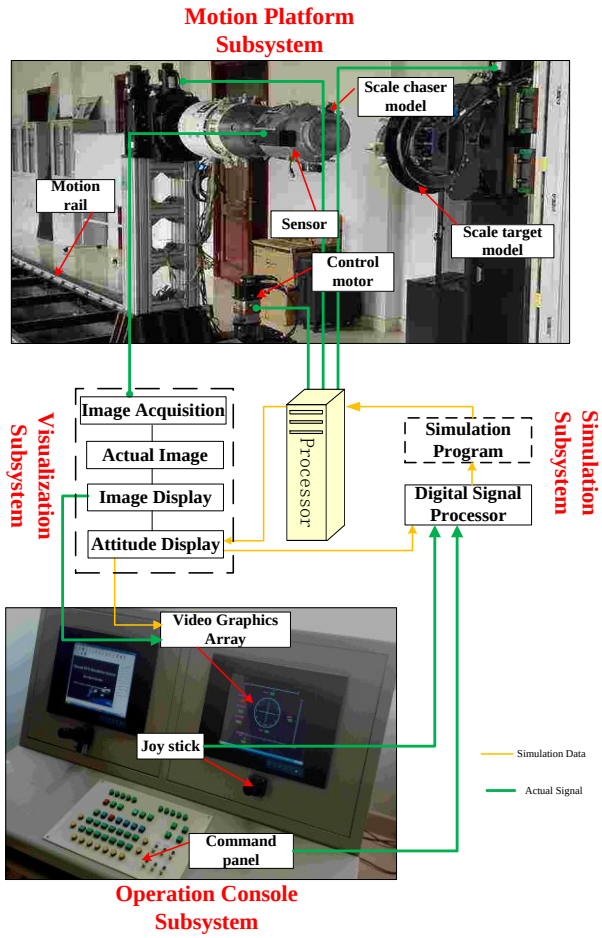

Figure 3 9-DOF manually controlled RVD platform

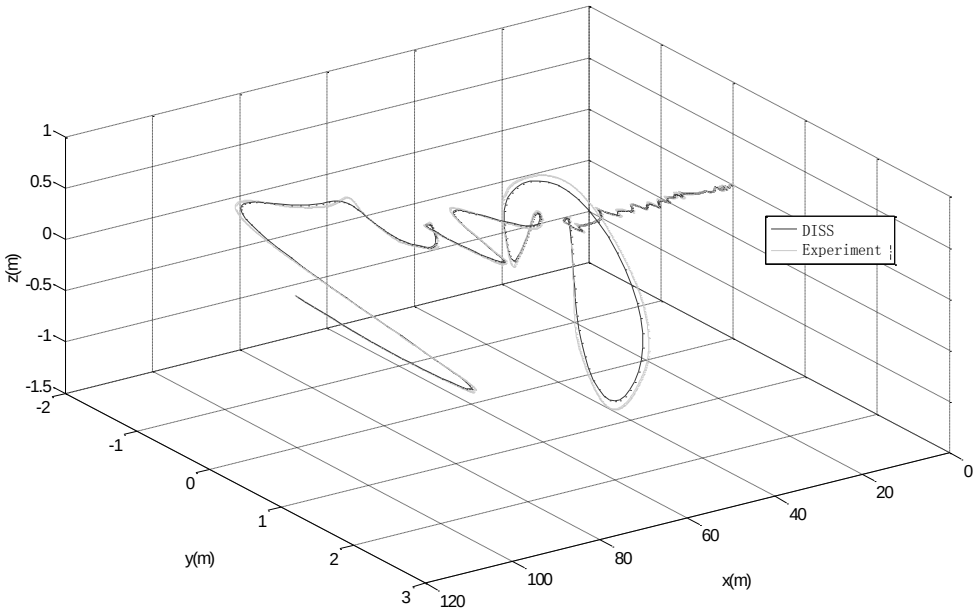

Figure 4 Manually controlled RVD trajectories in three dimensions, obtained by experiment and simulation

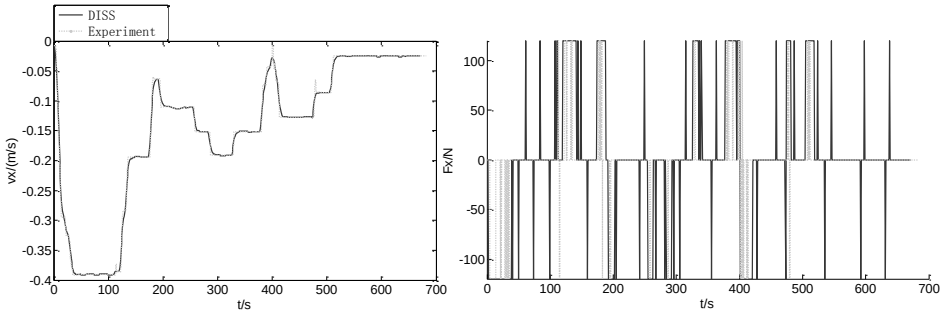

a. x-axis direction

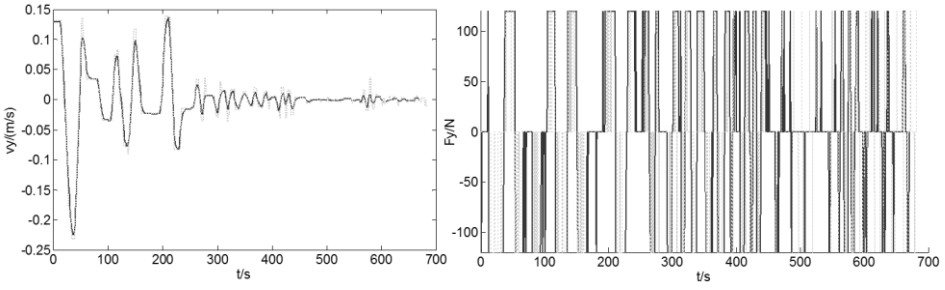

b. y-axis direction

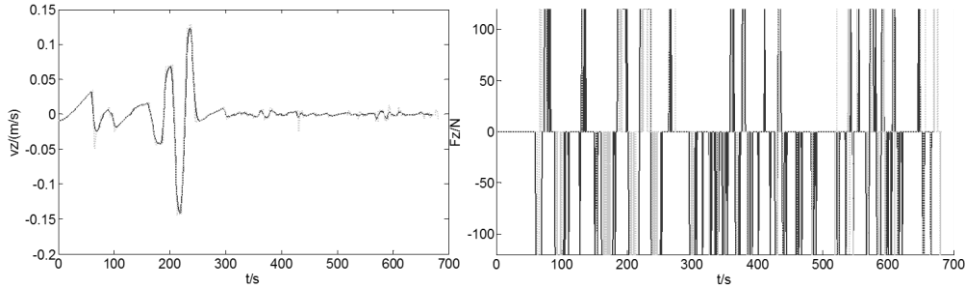

c. z-axis direction

Figure 5 Velocities and pulse amounts of manually controlled RVD

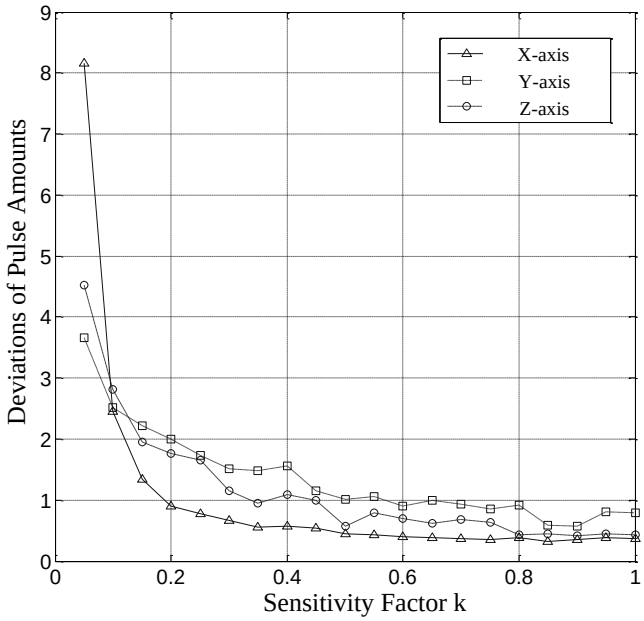

Figure 6 Average deviations of pulse amounts

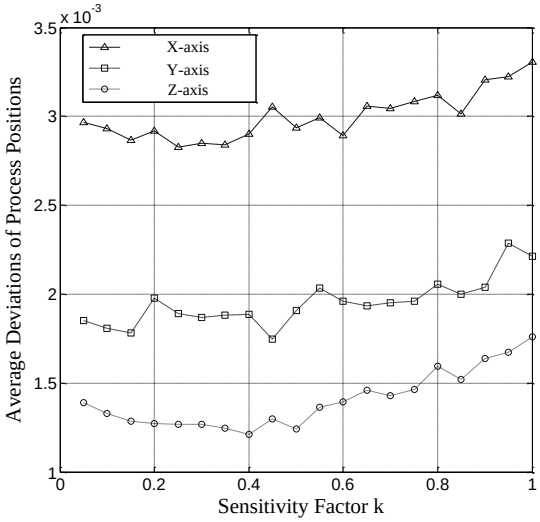

Figure 7 Average deviations of process positions

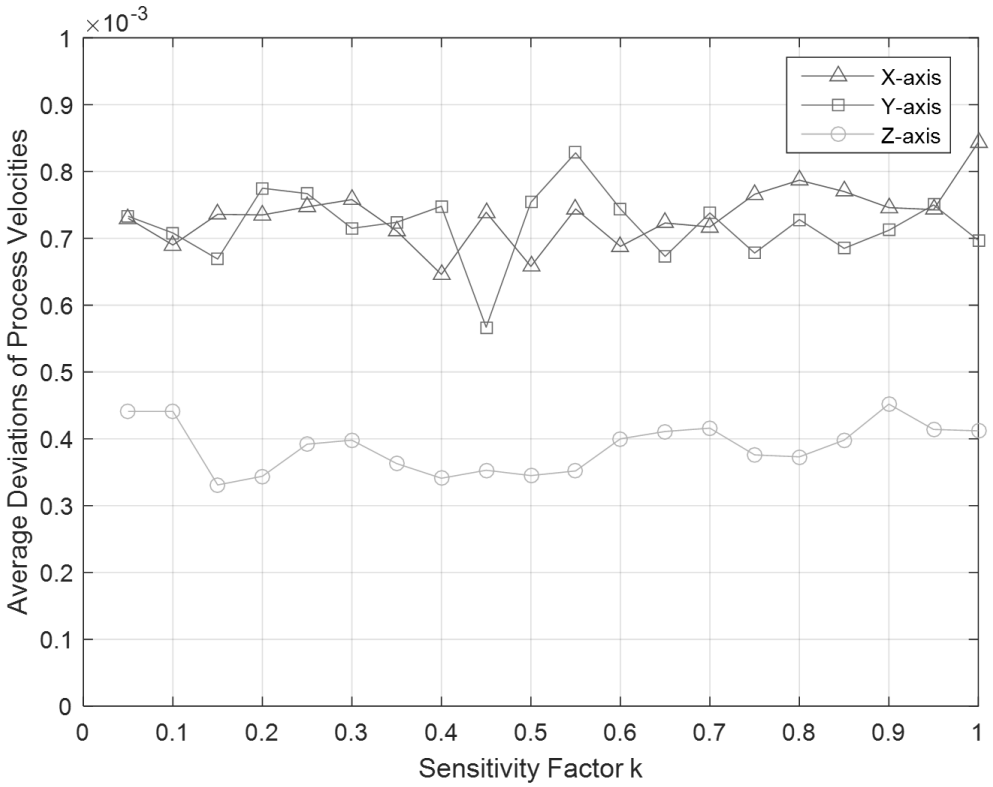

Figure 8 Average deviations of process velocities

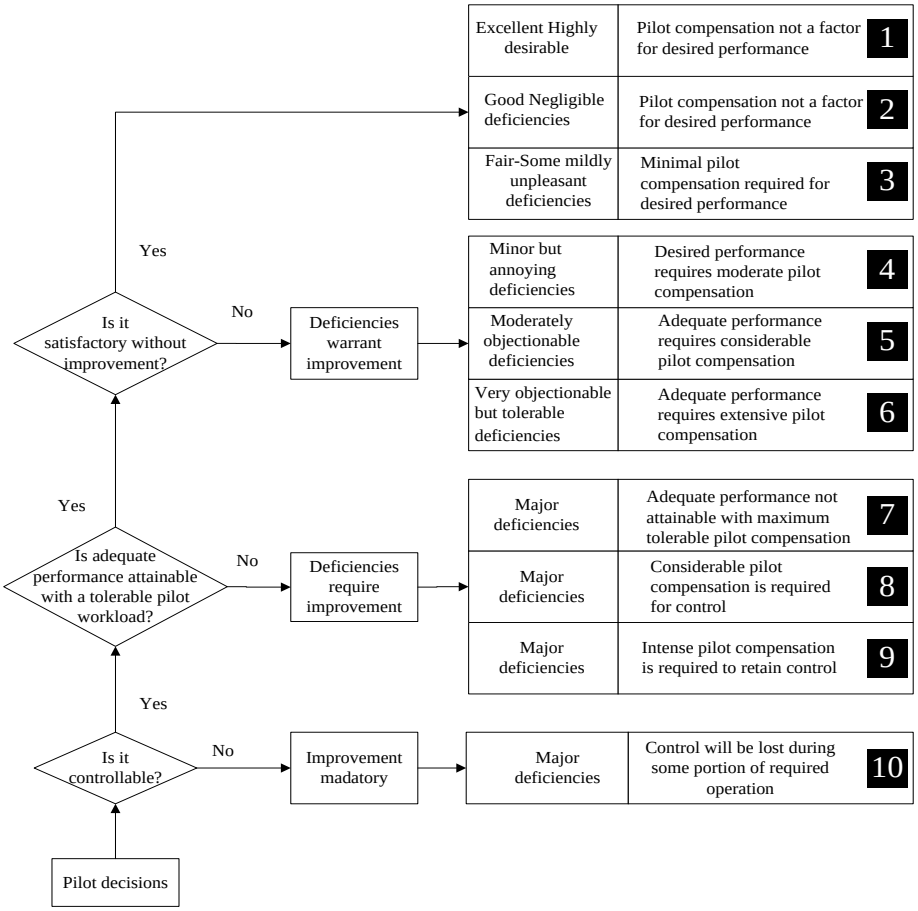

Figure 9 Cooper–Harper assessment ratings

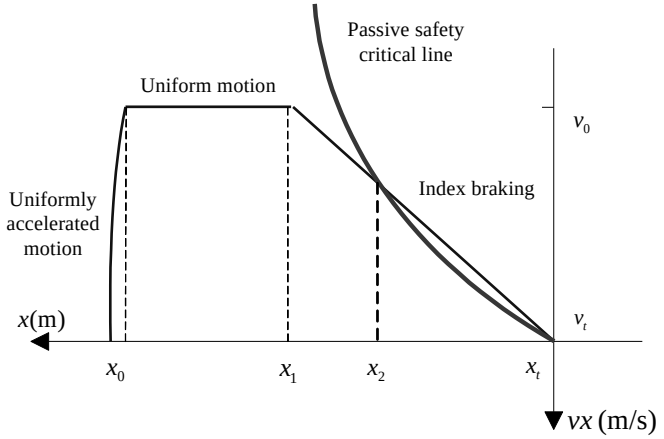

Figure 10 Guidance law combining active and passive safety modes

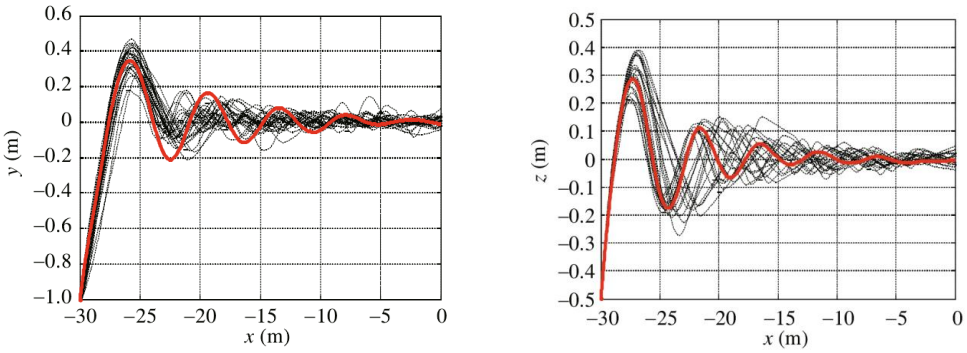

a. y-axis direction b. z-axis direction

Figure 11 Manually controlled nominal cross-track trajectories

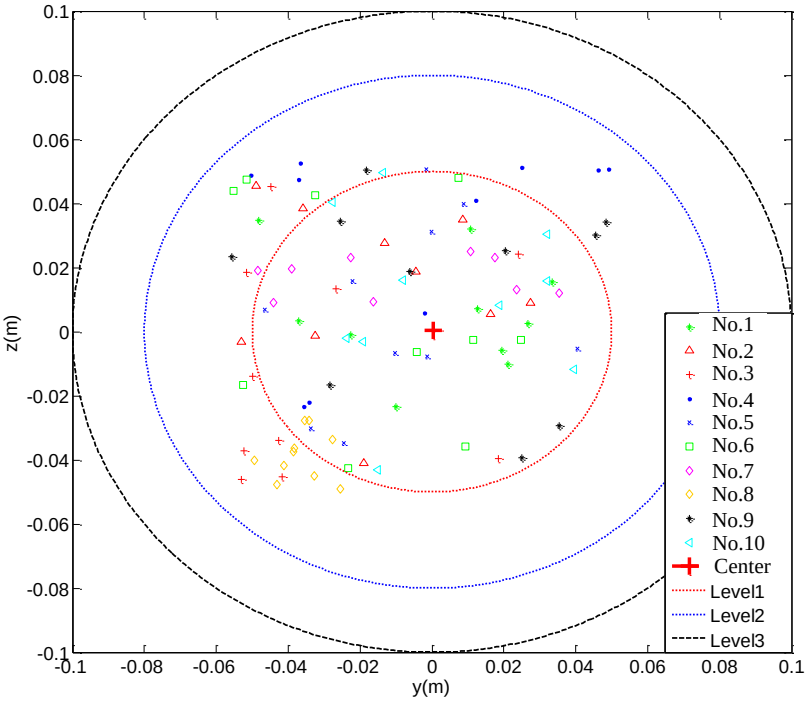

Figure 12 Impact distribution

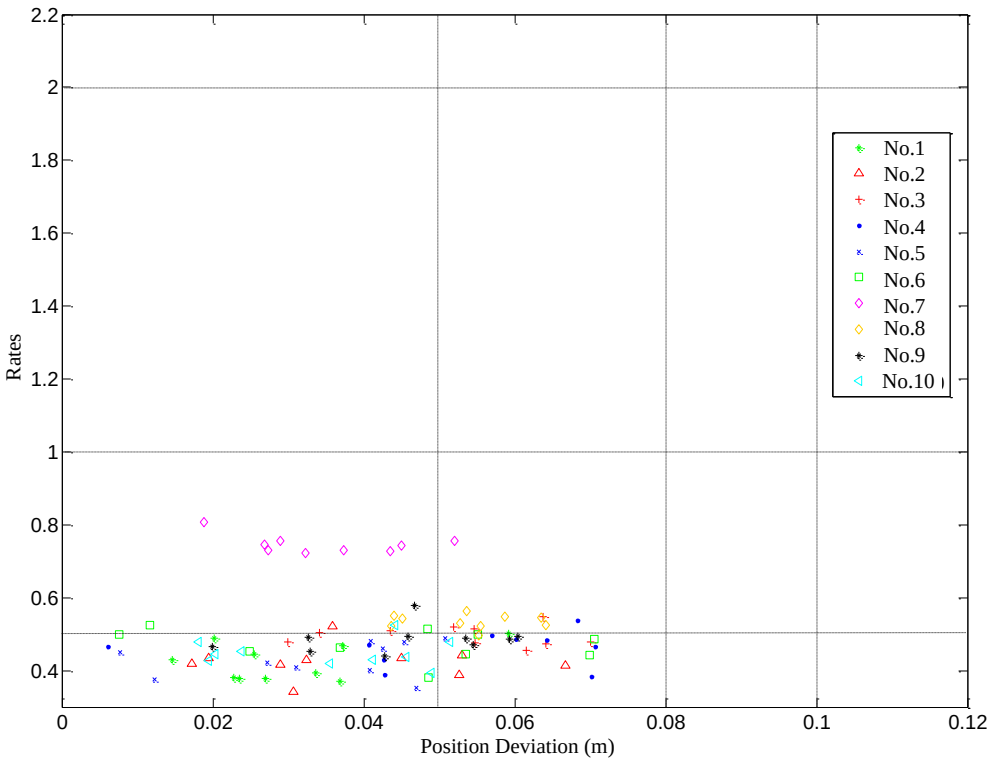

Figure 13 Handling qualities assessment for different trajectories